Supporting information

# *In Situ* Tuning of Magnetization and Magnetoresistance in $Fe_3O_4$ Achieved by All-Solid-State Redox Devices

*Takashi Tsuchiya,*[1,2]* *Kazuya Terabe,*[1] *Masanori Ochi,*[2] *Tohru Higuchi,*[2] *Minoru Osada,*[1] *Yoshiyuki Yamashita,*[1] *Shigenori Ueda,*[3,4] *and Masakazu Aono*[1]

[1]International Center for Materials Nanoarchitechtonics (WPI-MANA), National Institute for Materials Science (NIMS),1-1 Namiki, Tsukuba, Ibaraki 305-0044, Japan

[2]Department of Applied Physics, Faculty of Science, Tokyo University of Science, 6-3-1, Niijuku, Katsushika-ku, Tokyo 125-8585, Japan

[3]Quantum Beam Unit, National Institute for Materials Science (NIMS), 1-2-1 Sengen, Tsukuba, Ibaraki 305-0047, Japan

[4]Synchrotron X-ray Station at SPring-8, National Institute for Materials Science, 1-1-1 Kouto, Sayo, Hyogo 679-5148, Japan

**S1. Fabrication and characterization of all-solid-state redox transistor**

*S1.1 Fabrication of the device*

The all-solid-state redox transistor, schematically shown in **Fig. 1(a)**, was fabricated on an atomically flat (001) surface of undoped MgO single crystal. A 10-nm-thick $Fe_3O_4$ thin film was grown by pulse laser deposition (PLD) using a sintered stoichiometric $Fe_3O_4$ target pellet with 99.9% purity under a supply of pure nitrogen gas at a fixed flow rate of 1 sccm to maintain the adequate oxygen pressure. The substrate temperature was kept at 623 K during the deposition process. Then $Li_4SiO_4$ (LSO) thin film was deposited by using a sintered 20% Li excess LSO target pellet under a supply of pure oxygen gas at a fixed flow rate of 0.4 sccm to maintain the oxygen pressure at 0.2 Pa. The substrate temperature was kept at room temperature (RT) during the deposition process. The source and drain were made of a 60-nm-thick platinum thin films. These electrodes were deposited by RF sputtering with a metal mask at RT before LSO thin film was deposited. The channel length and width were 75 and 50 μm, respectively. 10 nm-thick titanium thin films were inserted as an adhesion layer at the source/$Fe_3O_4$ and drain/$Fe_3O_4$ interfaces. 20-nm-thick Tantalum oxide ($Ta_2O_5$) thin films were inserted to prevent charge accumulation at the Pt/LSO interface. The gate electrode was made of a 200-nm-thick $LiCoO_2$ thin film covered by a 100-nm-thick Pt thin film. Electrochemical measurements were performed in vacuum using a Keithley 4200-SCS parameter analyzer.

*S1.2 characterization of the $Fe_3O_4$ thin film*

The $Fe_3O_4$ was further assessed to be a single phase using Raman spectroscopy and X-ray photoemission spectroscopy shown in Fig. S1(a) and (b). Figure S1(a) shows Raman spectrum of the $Fe_3O_4$ thin film. Prominent structures A (670 $cm^{-1}$), B (530 $cm^{-1}$), and C (308 $cm^{-1}$) agree well with $A_{1g}$, $T_{2g}$ (2), and $T_{2g}$ (3) modes of $Fe_3O_4$ at room temperature.[r1] Figure S1(b) shows Fe 2p XPS spectrum of the $Fe_3O_4$ thin film. For reference, spectrum of $Fe_2O_3$ film is also shown. Structure A and B are Fe $2p_{3/2}$ emission for $Fe^{2+}$ and $Fe^{3+}$, respectively. Structure C, which is particularly significant for $Fe_2O_3$, is a charge transfer satellite mainly for $Fe^{3+}$.[r2] Structure A', B', and C' correspond to those for Fe $2p_{1/2}$ emission. Figure S1(c) shows resistivity of the $Fe_3O_4$ thin film as a function of temperature. $Fe_3O_4$ is known to show the Verwey transition at 120 K (Verwey temperature, $T_V$). A resistivity transition from a semiconducting to an insulating state occurs due to the transition. $T_V$ for the $Fe_3O_4$ thin film was estimated to be 108 K as a midpoint of two inflection points. $T_V$ of bulk $Fe_3O_4$ ($T_{V, Bulk}$) is also indicated for reference. The slight decrease in $T_V$ was found for the $Fe_3O_4$ thin film. Such $T_V$ decrease was well agree with the report for $Fe_3O_4$/MgO epitaxial thin films. The $T_V$ decrease was explained by strain due to the epitaxial growth on the substrate.[r3,4] Based on these observations, quality of the $Fe_3O_4$ film was confirmed.

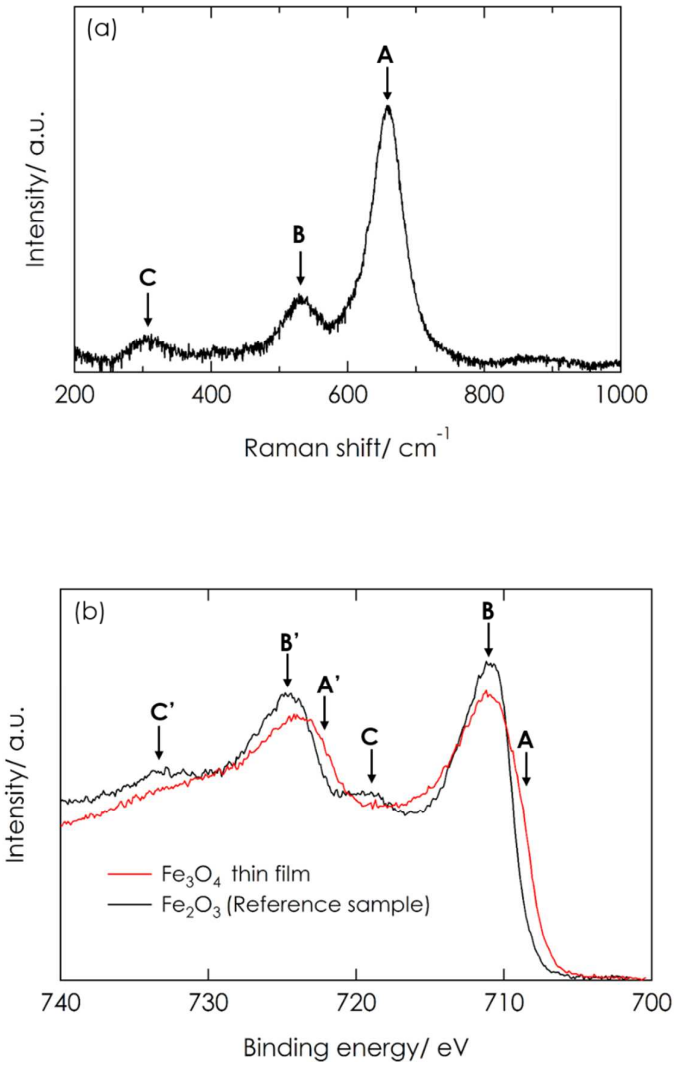


Figure S1(a) Raman spectrum and (b) X-ray photoemission spectrum of $Fe_3O_4$ thin film.

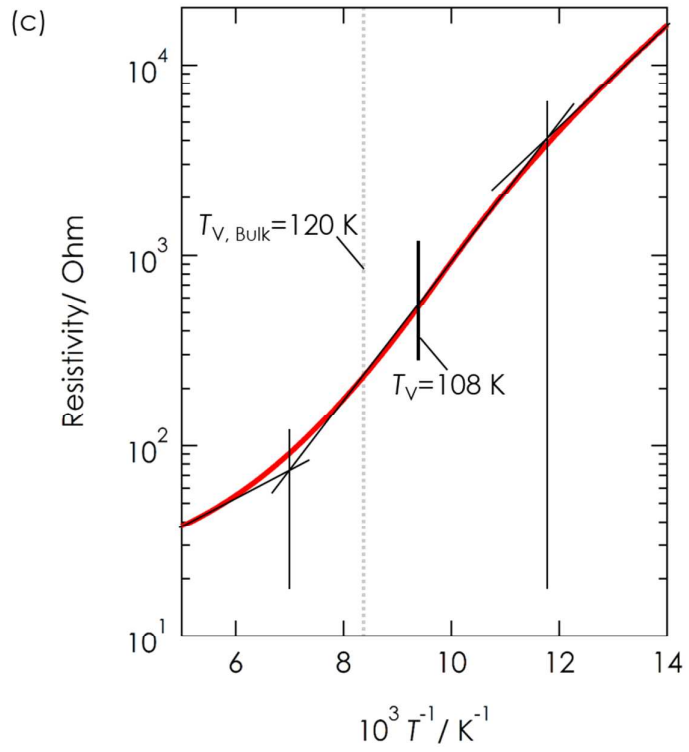


Figure S1(c) Resistivity as a function of temperature for $Fe_3O_4$ thin film. Verwey temperature ($T_V$) was estimated as a midpoint of two inflection points. $T_V$ of bulk $Fe_3O_4$ ($T_{V, Bulk}$) is indicated for reference.

**S2. $V_G$ Pulse response of the all-solid-state redox transistor**

$i_D/i_0$ can be reversibly switched by $V_G$ pulse below 2V. Figure S2 shows switching characteristics ($i_D/i_0$ *vs*. time) of the device for $V_G$ pulse of 2 V and 0 V with pulse width of 250 s. The device showed a reversible response due to the $Li^+$ insertion and removal although a response speed was comparably slow.

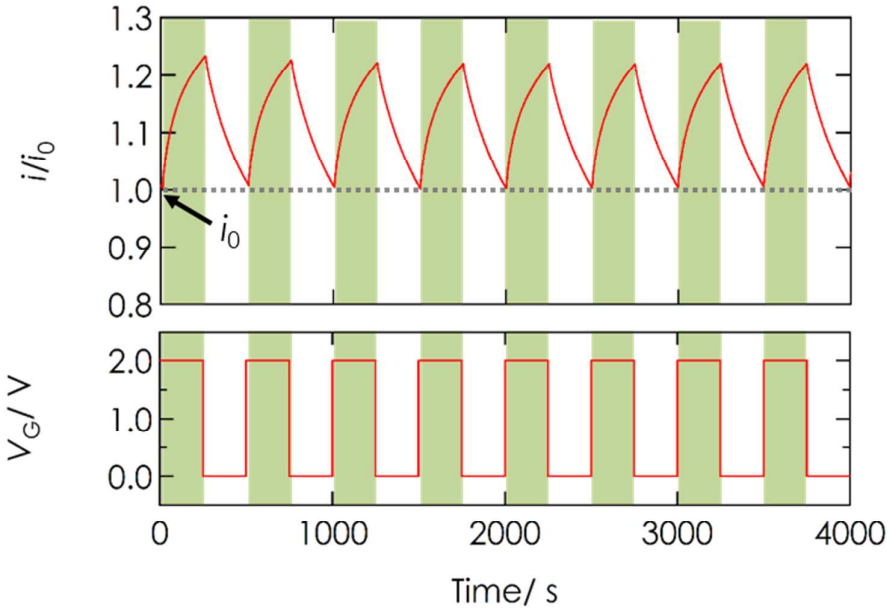


Figure S2. Switching characteristics ($i_D/i_0$ *vs*. time) of the device

**S3. Magnetic property modulation by $Li^+$ insertion**

*S3.1 Experiment procedure of MOKE measurement*

Magneto Optical Kerr effect (MOKE) measurement was performed to observe a magnetic property modulation in $Fe_3O_4$ caused by $Li^+$ insertion and removal achieved by an all-solid-state magnetic property tuning device. Setup for MOKE measurement is illustrated in Fig. S3(a). The device was prepared by a similar fabrication procedure (*e.g.* deposition methods for each films) as the redox transistor shown in Fig. 1(a). Thickness of the top Pt, $Fe_3O_4$, LSO, LCO, and bottom Pt films are 10, 30, 800, 200, 60 nm, respectively. The measurement was performed in polar Kerr configuration, where the magnetic field is normal to the thin film surface. Fig. S3(b) shows magneto-optical (MO) Kerr spectrum of the device measured under the magnetic field of 20 kOe. Linearly polarized light with a wavelength of 510 nm was used to measure $\theta_K$-$H$ loops. The measurement was performed in air at room temperature.

Figure S3(c) shows $\theta_K$-$H$ loop thick $Fe_3O_4$ (60 nm) reference sample. Typical ferromagnetic hysteresis of $Fe_3O_4$ was observed although the coercive field was slightly larger than thin $Fe_3O_4$ film (30 nm) in the all-solid-state device shown in Fig.S3 (a), indicating impact of thickness on domain wall behavior.

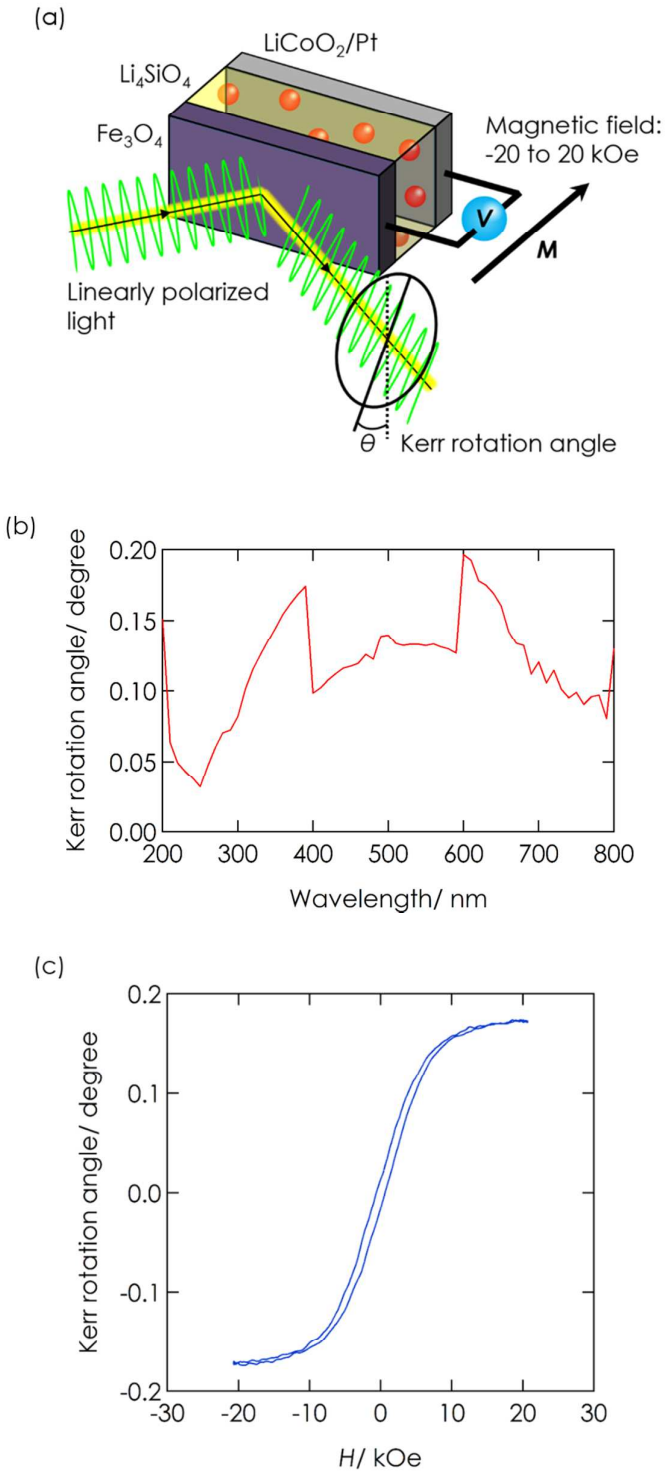


Figure 3(a) Illustration of setup for MOKE measurement. (b) $\theta_K$-$H$ loop thick $Fe_3O_4$ reference sample. (c) magneto-optical (MO) Kerr spectrum of the device measured under the magnetic field of 20 kOe.

*S3.2 M-H loops for chemically-lithiated $Fe_3O_4$ films measured by SQUID*

Impact of lithiation on magnetic property of $Fe_3O_4$ was further investigated by using $Fe_3O_4$ thin films lithiated by liquid reagent. First, magnetic property of 10 nm and 80 nm $Fe_3O_4$ thin films deposited on MgO(100) substrate were measured by Superconducting Quantum Interference Device (SQUID) magnetometry using Magnetic Property Measurement System (MPMS, Quantum Design, USA) at room temperature. The measurement was done in Reciprocating Sample Option (RSO) mode. Then, the samples were immersed in n-butyl-lithium in a dry box at 50 degree C for 72 hours and the magnetic property were measured again in the same set up as previous measurement. The lithiation procedure using n-butyl-lithium was described previously.[r5] *M-H* loops for 10 nm and 80 nm $Fe_3O_4$ thin films are shown in Fig. S3(d, e). Saturation *M* of lithiated $Fe_3O_4$ was decreased to 50 to 60% of $Fe_3O_4$ by a lithiation, although the extent of decrease was slightly different. Accordingly, decrease of *M* by lithiation was confirmed to be common phenomenon for both chemical and electrochemical methods. In addition, similar variation in magnetic property of $Fe_3O_4$ due to lithiation was observed by both SQUID and MOKE measurements.

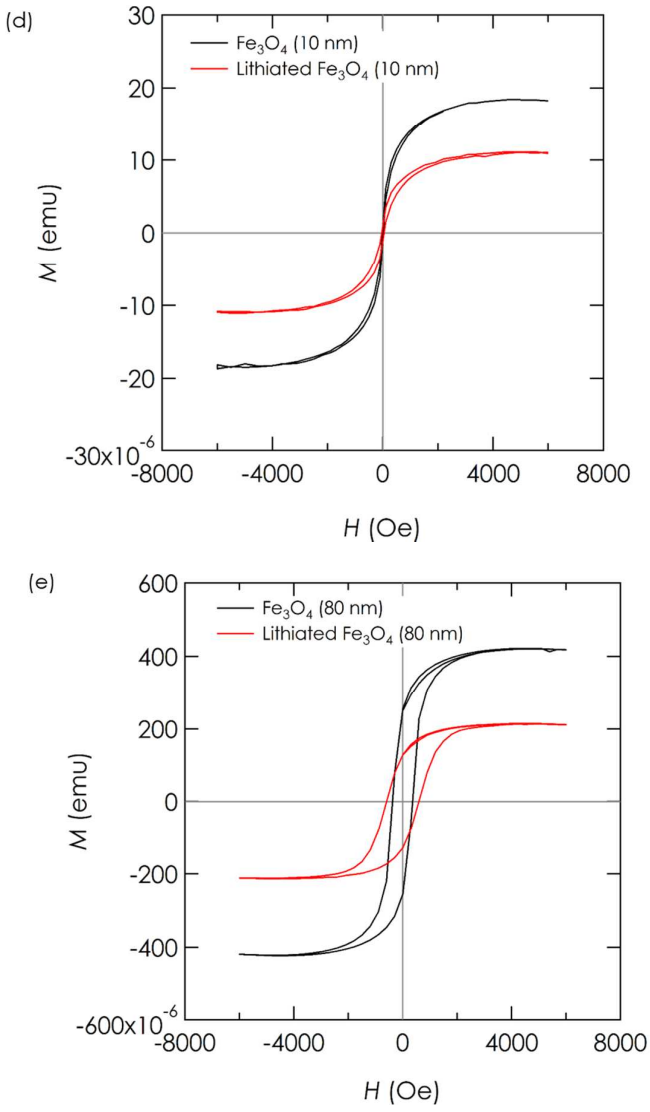


Figure S3 (d, e) *M-H* loops for $Fe_3O_4$ thin film before and after lithiation measured by SQUID. (d) and (e) are for 10 nm and 80 nm thick $Fe_3O_4$ thin films.

*S3.3 Cycling property of magnetic property tuning*

Cycling property of magnetic property tuning of the device shown in Fig. S3(a) was investigated by repeating DC voltage application. First, 0 V was applied for 1000 s and $\theta_K$ -*H* loop was measured. Subsequently, 2 V was applied for 1000 s and $\theta_K$ -*H* loop was measured. The whole cycle was repeated for 4 times. The saturation *M* (*i.e.* $\theta_K$) showed comparably good repeatability although saturation *M* slightly deviated from time to time.

*S3.4 Magnetoresistance tuning in the all-solid-state redox transistor*

Variation of magnetoresistance (MR) in the all-solid-state redox device shown in Fig. 1(a) was measured using Physical Property Measurement System (PPMS, Quantum Design, USA). The measurement was performed in helium gas flow at 250 K, at which resistance fluctuation while the MR measurement, which is originated from ion migration, can be extremely small. First, 0 V was applied for 1000 s at 298 K and then the device was cooled down to 250 K with the DC voltage applied, followed by the MR measurement in the magnetic field from -70 kOe to 70 kOe. After the MR measurement was finished, the device was heat up to 298 K. The cycle was repeated with increasing DC voltage from 0 to 4 V by 0.5 V step.

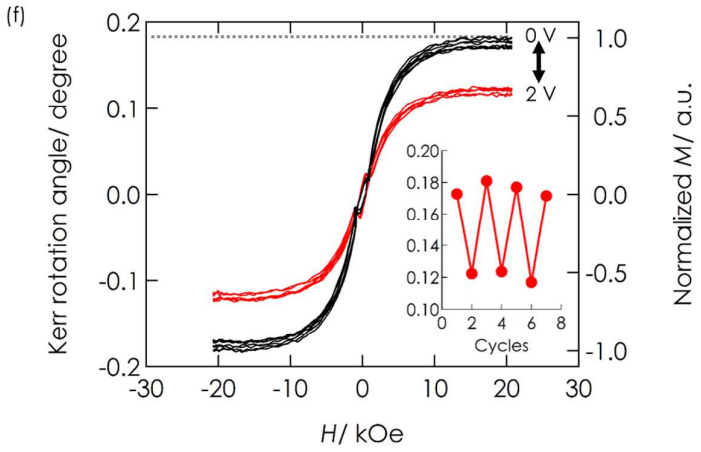


(f) $\theta_K$ -*H* loops of the all-solid-state magnetic property tuning device observed in 0 V and 2 V application cycles. Inset shows saturation $\theta_K$ for each cycles.

**S4. Experimental procedure of *in-situ* hard X-ray photoelectron spectroscopy**

*S4.1 Fabrication procedure of the device*

The two-terminal electrochemical cell, schematically shown in Fig. S4(a), was fabricated on an atomically flat (001) surface of undoped MgO single crystal. A 60-nm-thick Pt and a 200-nm-thick $LiCoO_2$ thin films were deposited by RF sputtering method. Then $Li_4SiO_4$ (LSO) thin film was deposited by using a sintered 20% Li excess LSO target pellet under a supply of pure oxygen gas at a fixed flow rate of 0.4 sccm to maintain the oxygen pressure at 0.2 Pa. The substrate temperature was kept at room temperature (RT) during the deposition process. A 30-nm-thick $Fe_3O_4$ thin film was grown by pulse laser deposition (PLD) using a sintered stoichiometric $Fe_3O_4$ target pellet with 99.9% purity under a supply of pure nitrogen gas at a fixed flow rate of 1 sccm to maintain the adequate oxygen pressure. The substrate temperature was kept at 623 K during the deposition process. A 5-nm-thick Pt was deposited by electron beam (EB) deposition method. The $Fe_3O_4$ and top Pt thin films were deposited to the dimensions of $3\times3$ $mm^2$ with a help of a metal mask.

*S.4.2 in-situ HX-PES measurement procedure*

HX-PES measurement was performed at the beam line BL-15XU of SPring-8 synchrotron radiation facility in Japan. The overall resolution of the instrument estimated is 0.15 eV at 5948 eV of photon energy while the binding energy values are referenced to the metallic Au Fermi edge. The present measurements were performed using the excitation by hard X-ray source at an incident angle of 82 degree, which can penetrate to micrometer range, and the detection of photoelectron with an escape depth of 10-20 nm.[33-39] All HX-PES measurement was conducted in a high vacuum, typically $7.0\times10^{-8}$ Pa.

DC voltage dependence of HX-PES spectra of the device shown in Fig. 3 was investigated with DC voltage applied condition. The applied DC voltage was changed as 0, 1, 2, 3, 0 V for the first cell and the result is shown in Figs. 3(a, b). For example, 0 V was applied for 1000 s at first and the HX-PES measurement was performed. Subsequently, the applied voltage was increased to 1 V and kept for 1000 s, followed by the HX-PES measurement. For the second cell which was prepared in the same batch as the first cell, the applied voltage was changed as 0, 2, 0 V, and the result is shown in Figs. 3(c, d).

In addition to Fe 2s HX-PES spectra shown in Figs. 3, Pt 4f spectra of the top Pt film were measured to check possible peak shift (Fermi level shift) due to experimental errors including charge up of the electrode and unexpected IR drop in a lead. Figures S4 (b, c) show the Pt 4f spectra measured simultaneously with Fe2s spectra shown in Figs. 3 (a, c). Through the experiment, considerable peak shift in both Pt $4f_{5/2}$, and Pt $4f_{7/2}$ core levels was not observed, ruling out undesired contribution from experimental errors (Fermi level shift). The variation in Fe 2s peak

shape shown in Figs. 3 was attributed to valence change in $Fe_3O_4$ accordingly.

*S.4.3 Fe 2s spectra of reference iron oxide samples.*

For reference of the analysis of Fe 2s spectra, Fe 2s spectra of iron oxides of $Fe_2O_3$ ($Fe^{3+}$) and FeO ($Fe^{2+}$) thin films were measured using electron spectroscopy for chemical analysis (ESCA) with Mg X-ray source. The Fe 2s spectra were shown in Fig. S4(d). The peak binding energy of $Fe_2O_3$ and FeO were 849.8 and 848.3 eV, respectively. The observed binding energy of $Fe_2O_3$ slightly larger than that (849.0 eV) reported previously.[r6] The energy difference of 1.6 eV is close to that (1.7 eV) in Fe 3s for $Fe_2O_3$ ($Fe^{3+}$) and FeO ($Fe^{2+}$).[r7,8] Both the spectra of iron oxides show much broader peak shape than HX-PES spectra shown in Figs. 3 due to broad Mg K-$\alpha$ line.

*S. 4.4 Deconvolution of Fe2S HX-PES spectra using multi peak fitting*

Deconvolution of Fe 2s HX-PES spectra was performed using multi peak fitting method to calculate amount of $Fe^{3+}$ and $Fe^{2+}$ ions in $Fe_3O_4$ under DC voltage applied condition. Modified Gaussian function was used for asymmetric Fe2s peaks.[r9,10] The function is expressed as

$$f(x) = \frac{\text{Peak height}}{\exp\left\{\frac{4}{\Gamma^2}\ln(2)(x-x_0)^2 \Big/ \left\{1+\alpha(x-x_0)/\Gamma\right\}^2\right\}} \qquad (1)$$

, where $x_0$, $\alpha$, and $\Gamma$ are peak position, asymmetric parameter ($-2<\alpha<2$), and peak width, respectively.

At first, Fe 2s HX-PES spectrum at 0 V shown in Fig. 3(a) was analyzed by sum of the functions (1) for $Fe^{3+}$ and $Fe^{2+}$ ions assuming that $\alpha$ is common for the functions (1) for $Fe^{3+}$ and $Fe^{2+}$ ions and peak height ratio ($Fe^{3+}$:$Fe^{2+}$) at 0 V is 2:1 (corresponding to stoichiometric $Fe_3O_4$). $x_0$ for $Fe^{3+}$ and $Fe^{2+}$ ions were fixed at 849.8 and 848.3 eV obtained by ESCA measurement described in S 4.3. Calculation result is shown in Fig. S4(e). $\alpha$ was thus calculated as 0.493 (<2).

The $\alpha$ value was used for subsequent analysis of the other Fe 2s spectra under various DC voltage conditions shown in Fig. 3(a). For the analysis, peak height ratio and $\Gamma$ were put as fitting parameter and the obtained $Fe^{3+}$:$Fe^{2+}$ was shown in Fig. 3(b). The same analysis procedure was performed for the Fe 2s HX-PES spectra shown in Fig. 3(c). $\alpha$ was calculated as 0.555 (<2) for the case.

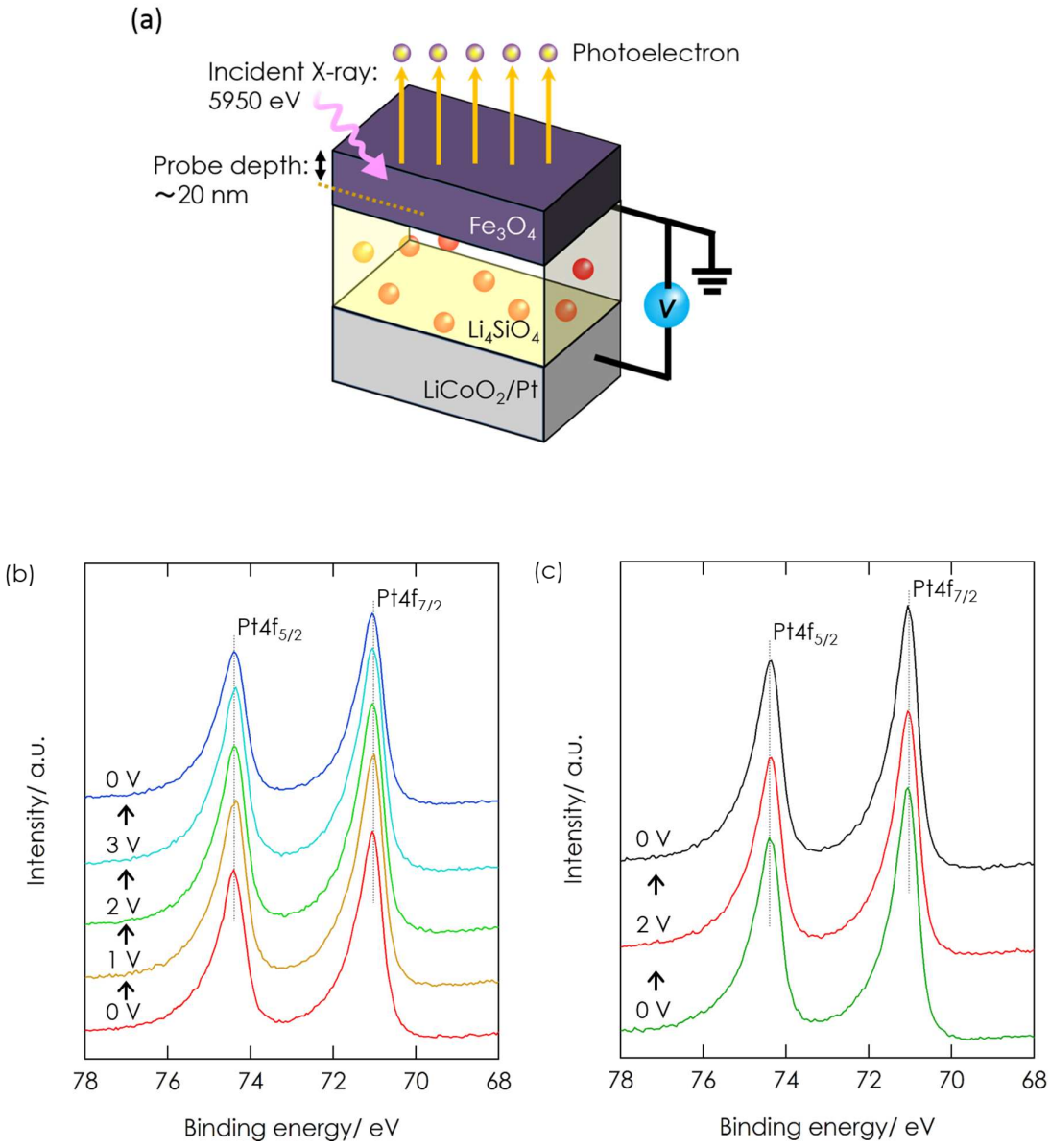


Figure S4 (a) Illustration of two terminal set up for in situ HX PES measurement. (b, c) Pt 4f spectra measured simultaneously with Fe 2s shown in Figs. 3 (a, c).

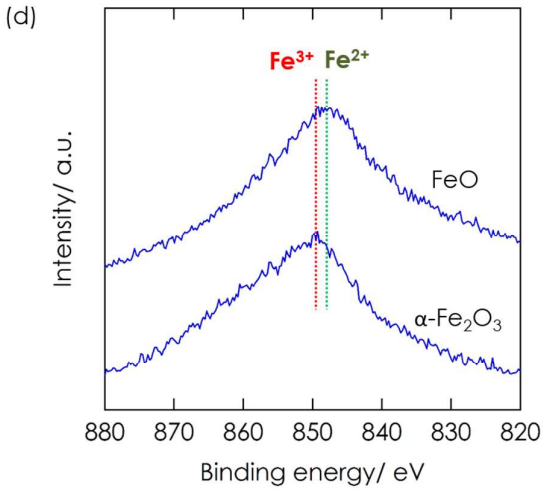


Figure S4 (d) ESCA spectra of $Fe_2O_3$ ($Fe^{3+}$) and FeO ($Fe^{2+}$) thin films measured for reference of HX-PES.

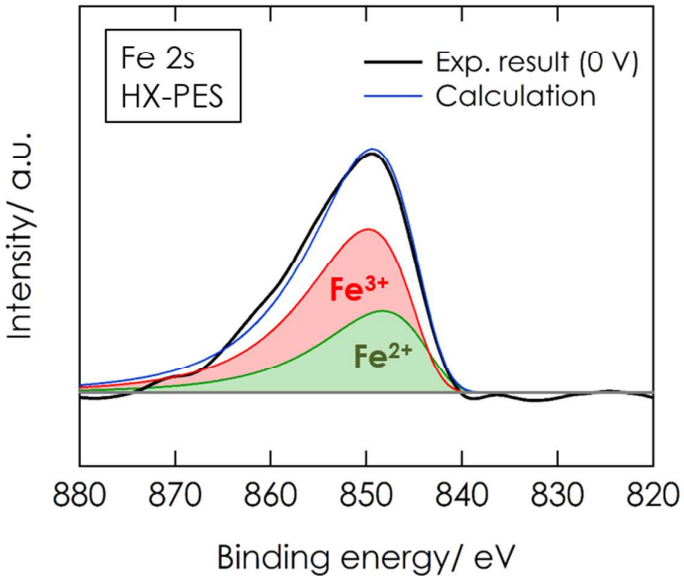


Figure S4 (e) An Example of multi peak fitting for Fe 2s HX-PES spectrum of 0 V shown in Fig. 3(a). Red, green, and blue curves are $Fe^{3+}$, $Fe^{2+}$, and sum of the two components calculated by the fitting.

Reference

(r1) Phase, D. M.; Tiwari, S.; Prakash, R.; Dubey, A.; Sathe, V. G.; Choudhary, R. J., Raman Study across Verwey Transition of Epitaxial $Fe_3O_4$ Thin Films on MgO (100) Substrate Grown by Pulsed Laser Deposition, *J. Appl. Phys.*, **2006**, *100,* 123703

(r2) Fujii, T.;. de Groot, F. M. F.; Sawatzky, G. A.; Voogt, F. C.; Hibma, T.; Okada, K., *In Situ* XPS Analysis of Various Iron Oxide Films Grown by $NO_2$-Assisted Molecular-Beam Epitaxy, *Phys. Rev. B*, **1999**, *59*, 3195 -3202

(r3) Orna, J.; Algarabel, P. A.; Morellón, L.; Pardo, J. A.; de Teresa, J. M.; López Antón, R.; Bartolomé, F.; García, L. M.; Bartolomé, J.; Cezar, J. C.; Wildes, A., Origin of the Giant Magnetic Moment in Epitaxial $Fe_3O_4$ Thin Films, *Phys. Rev. B*, **2010**, *81*, 144420

(r4) Li, X. W.; Gupta, A.; Xiao, G.; Gong, G. Q., Transport and Magnetic Properties of Epitaxial and Polycrystalline Magnetite Thin Films, *J. Appl. Phys*., **1998**, *83,*7049

(r5) Thackey, M.M.; David, W.I.F.; Goodenough, J.B., Structural Characterization of the Lithiated Iron Oxides $Li_xFe_3O_4$ and $Li_xFe_2O_3$ ($0<x<2$), *Mat. Res. Bull.* **1982**, *17*, 785-793

(r6) Allen, G. C.; Curtis, M. T.; Hooper, A. J.; Tucker, P. M., X-ray Photoelectron Spectroscopy of Iron–Oxygen Systems, *J. Chem. Soc. Dalton Trans*. **1974**, 1525

(r7) Mills, P.; Sullivan, J. L., A Study of the Core Level Electrons in Iron and Its Three Oxides by Means of X-ray Photoelectron Spectroscopy, *J. Phys. D.* **1983**, *16*, 723

(r8) McIntyre, N. S.; Zetaruk, D. G., X-ray Photoelectron Spectroscopic Studies of Iron Oxides, *Anal. Chem*. **1977**, *49*, 1521

(r9) Ansell, R. O.; Dickson, T.; Povey, A. F.; Sherwood, P. M. A., X-ray Photoelectron Spectroscopic Studies of Electrode Surfaces Using a New Controlled Transfer Technique: Part 2. Results for a Molybdenum Electrode and the Curve Fitting Procedure, *J. Electroanal. Chem*., **1979**, *98*, 79

(r10) Kojima, I.; Fukumoto, N.; Kurahashi, M., Analysis of X-ray Photoelectron Spectrum with Asymmetric Gaussian-Lorentzian Mixed Function, *Bunseki Kagaku*, **1986**, *35*, 96-100